Energy &
Environmental Science

Cite this: *Energy Environ. Sci.*, 2011, **4**, 1364

www.rsc.org/ees

PAPER

Facile preparation and enhanced photocatalytic H_2-production activity of $Cu(OH)_2$ cluster modified TiO_2

Jiaguo Yu* and Jingrun Ran

Received 1st December 2010, Accepted 3rd February 2011
DOI: 10.1039/c0ee00729c

$Cu(OH)_2$ cluster-modified TiO_2 ($Cu(OH)_2/TiO_2$) photocatalysts were prepared by a simple precipitation method using Degussa P25 TiO_2 powder (P25) as a support and copper nitrate as a precursor. Low-power ultraviolet light emitting diodes (UV-LEDs) were used as the light source for a photocatalytic water splitting reaction. The prepared samples show especially high photocatalytic H_2-production activity from aqueous solutions containing ethylene glycol as sacrificial reagent even without a Pt co-catalyst. The optimal $Cu(OH)_2$ loading content was found to be 0.29 mol%, giving an H_2-production rate of 3418 μmol h^{-1} g^{-1} with a quantum efficiency (QE) of 13.9%, which exceeded the rate on pure TiO_2 by more than 205 times. This high photocatalytic H_2-production activity is attributed to the presence of $Cu(OH)_2$ clusters on the surface of the TiO_2. The potential of $Cu(OH)_2/Cu$ ($Cu(OH)_2 + 2e^- = Cu + 2OH^-$, $E^o = -0.224$ V) is slightly lower than conduction band (−0.26 V) of anatase TiO_2, whilst being higher than the reduction potential of H^+ ($2H^+ + 2e^- = H_2$, $E^o = -0.000$ V), which favors the electron transfer from the CB of TiO_2 to $Cu(OH)_2$, and the reduction of H^+, thus enhancing photocatalytic H_2-production activity. This work not only shows a possibility for the utilization of low cost $Cu(OH)_2$ clusters as a substitute for noble metals (such as Pt) in photocatalytic H_2-production, but also for the first time exhibits a facile method for enhancing H_2-production activity by using hydroxide as a co-catalyst .

1. Introduction

Fossil fuels, such as coal, oil and natural gas, are non-renewable energy sources which play a crucial role in the quality of life of human beings and in the development of the world economy. However, combustion of fossil fuels causes a series of crises surrounding global energy and environment. Therefore, development of clean and renewable energy sources has attracted much attention and has become a significant development strategy in most countries.[1]

Hydrogen energy is an ideal candidate for the replacement of fossil fuels in the future because of its high-energy capacity, environmental friendliness, and recycling possibility.[2] The idea of capturing solar energy that is freely available from sunlight and converting it into hydrogen energy has been considered to be an attractive and meaningful route for solar energy conversion. As a sustainable approach for hydrogen production, photocatalytic

State Key Laboratory of Advanced Technology for Material Synthesis and Processing, Wuhan University of Technology, Luoshi Road 122#, Wuhan, 430070, P. R. China. E-mail: jiaguoyu@yahoo.com; Fax: (+86)-27-87879468; Tel: (+86)-27-87871029

Broader context

Hydrogen energy is an ideal candidate for the replacement of fossil fuels in the future. As a sustainable approach for hydrogen production, photocatalytic water splitting using semiconductor photocatalysts is a promising way to achieve hydrogen generation. However, the H_2-production efficiency of photocatalytic water splitting over bare titania remains quite limited. Both the deposition of noble metals on the titania surface and the addition of sacrificial reagents (electron donors or hole scavengers) into reaction solutions have been intensively explored for photocatalytic hydrogen production. Here we report the fabrication of $Cu(OH)_2$ cluster-modified TiO_2 photocatalysts by a facile precipitation method, and examine the resulting photocatalyst for hydrogen production using an industrial by-product, ethylene glycol, as a sacrificial reagent. This was proven to be an effective electron donor in photocatalytic water splitting, and it is a common industrial waste originating from some chemical processes. This work not only shows a possibility for the utilization of low cost $Cu(OH)_2$ clusters as a substitute for noble metal Pt in photocatalytic H_2-production but also exhibits a facile method for enhancing H_2-production activity by using hydroxide as a co-catalyst, also confirming that photocatalytic hydrogen production and the decomposition of pollutants occurred simultaneously.

water splitting using semiconductor photocatalysts is a promising and useful way for hydrogen generation since the discovery of photocatalytic splitting of water on TiO_2 electrodes in 1972 by Honda and Fujishima.[3–9] In comparison to other semiconductor photocatalysts, TiO_2 is a suitable material described as a photocatalyst for water splitting because of its biological and chemical inertness, cost-effectiveness, environmental friendliness, availability, long-term stability against photo- and chemical-corrosion, and especially its energy band edges which are well-matched with the redox potentials of water.[10–14]

However, the H_2-production efficiency of photocatalytic water splitting over bare nano-sized titania remains quite limited, mainly due to the high recombination rate of photogenerated CB electrons and VB holes.[15] To resolve this problem, many methods have been proposed to enhance the photocatalytic activity of TiO_2, such as noble metal loading,[16–19] metal ion doping,[20–22] carbon and nitrogen doping,[23,24] dye sensitization,[25,26] and also addition of sacrificial reagents (electron donors or hole scavengers).[27–29] The principal methods of inhibiting the CB electron and VB hole recombination are deemed to be through the loading of metal co-catalysts onto the surface of the TiO_2 and the addition of sacrificial reagents to the reaction system.

To achieve an efficient photocatalytic H_2-production rate, addition of specific chemicals as hole scavengers (sacrificial reagents) into photocatalytic systems can inhibit photogenerated CB electron and VB hole recombination. However, it is obviously meaningless to use sacrificial reagents such as methanol or ethanol for hydrogen generation, because they are already good fuels. In comparison, the utilization of organic pollutants or industrial waste as sacrificial reagents, followed by decomposing them into environmentally friendly products, has been identified as a clean and economical method.[30,31] For example, ethylene glycol is produced in large amounts as industrial and civil waste,[32–34] and has been proven to be an effective electron donor for photocatalytic hydrogen generation.[35]

On the other hand, for effective H_2-production, noble metals, such as Pt,[30] Au[31] and Pd,[36] must be used in most photocatalytic systems as a co-catalyst loaded onto the surface of TiO_2 to promote the separation and transfer of charge carriers from the TiO_2 to the loaded noble metals where H^+ is reduced to hydrogen molecules. Among various metals, loading of Pt onto the TiO_2 surface has proven to show a higher efficiency for photocatalytic water splitting in the presence of sacrificial reagents. However, Pt is both expensive and rare. Therefore, more research has been undertaken to identify low cost co-catalysts with acceptable enhancement of photocatalytic activity.[10]

Cu-containing TiO_2 has proven to be a cost-effective and efficient photocatalyst for hydrogen production.[16,18,37,38] For example, Sreethawong *et al.*[39] reported that, compared to Ni, Cu showed a two times higher enhancement of TiO_2 activity for hydrogen production. Bandara *et al.*[15] and Choi *et al.*[40] synthesized CuO incorporated TiO_2 and found that hydrogen generation was greatly improved by CuO compared to pure TiO_2. Xu *et al.*[41] reported that Cu incorporated TiO_2 was more efficient than some Pt loaded TiO_2 for hydrogen production. However, the above studies mainly focus on the photocatalytic behavior of CuO or Cu_2O modified TiO_2 for hydrogen production. To our knowledge, there is no report on $Cu(OH)_2$ clusters as co-catalysts for photocatalytic H_2-production. In this paper, the deposition of $Cu(OH)_2$ clusters on the surface of TiO_2 was achieved by a facile precipitation method using P25 as a support, and $Cu(NO_3)_2$ and NaOH as a precursors. Ethylene glycol was used as a sacrificial reagent and low power UV-LEDs were used as the light source for photocatalytic H_2-production.

2. Experimental

2.1 Sample preparation

All the reagents were of analytical grade and were used without further purification. Deionized water was used in all experiments. Commercially available Degussa P25 TiO_2 powder (P25) was used as the source of TiO_2. $Cu(OH)_2/TiO_2$ photocatalysts were prepared by a simple precipitation method. In a typical synthesis, 0.4 g of P25 was dispersed in 50 ml of 0.25 M NaOH aqueous solution, and then a certain volume of 0.0077 M $Cu(NO_3)_2$ aqueous solution was added dropwise under stirring. The mixed solutions were stirred for 6 h at room temperature. After that, the precipitates were washed with deionized water and ethanol five times. Finally, the washed precipitates were dried at 80 °C for 12 h. The nominal molar ratios of $Cu(OH)_2$ to (TiO_2 + $Cu(OH)_2$), which hereafter is designated as $\boldsymbol{R}$, were 0, 0.05, 0.25, 1, 2, and 7 nominal mol. % (mol%) (see Table 1), and the resulting samples were labeled as C0, C0.05, C0.25, C1, C2, and C7, respectively. The actual chemical compositions of the prepared samples were measured by inductively coupled plasma atomic emission spectrometry (ICP-AES) using an Optima 4300 DV spectrometer (Perkin Elmer) (see Table 1). Pure $Cu(OH)_2$ was also prepared for the purpose of comparison under the same experimental conditions, and the resulting $Cu(OH)_2$ sample was labeled as C100.

2.2 Characterization

X-Ray diffraction (XRD) patterns, obtained on an X-ray diffractometer (Rigaku, Japan) using Cu Kα irradiation at a scan rate of $0.05^\circ\ 2\theta\ s^{-1}$, were used to determine the phase structures of the obtained samples. The accelerating voltage and applied current were 40 kV and 80 mA, respectively. The average crystallite size was calculated using the Scherrer formula ($d = 0.9\lambda/B\cos\theta$, where d, λ, B and θ are crystallite size, Cu Kα wavelength (0.15418 nm), full width at half maximum intensity (FWHM) in radians and Bragg's diffraction angle, respectively), after correcting the instrumental broadening. Transmission electron microscopy (TEM) analyses were conducted on a JEM-2100F electron microscope (JEOL, Japan), using a 200 kV accelerating voltage. The Brunauer–Emmett–Teller (BET) specific surface area (S_{BET}) of the powders was analyzed by nitrogen adsorption in a Micromeritics ASAP 2020 nitrogen adsorption apparatus (USA). All of the as-prepared samples were degassed at 180 °C prior to nitrogen adsorption measurements. The BET surface area was determined by a multipoint BET method using adsorption data in the relative pressure (P/P_0) range of 0.05–0.3. A desorption isotherm was used to determine the pore size distribution *via* the Barret–Joyner–Halender (BJH) method, assuming a cylindrical pore model. The nitrogen adsorption volume at a relative pressure (P/P_0) of 0.994 was used to determine the pore volume and average pore size. UV-vis diffused reflectance spectra of the samples were obtained for the dry-pressed disk samples on a UV-vis spectrophotometer (UV2550, Shimadzu, Japan). $BaSO_4$ was used as a reflectance standard in a UV-vis diffuse reflectance

Table 1 Effects of ***R*** on the physicochemical properties and QE of $Cu(OH)_2/TiO_2$ samples

Samples	***R***	$Cu(OH)_2$ (mol.%) (ICP-AES)	ACS [a] (nm)	S_{BET} ($m^2\ g^{-1}$)	PV [b] ($cm^3\ g^{-1}$)	Porosity (%)	QE (%)
C0	0	0	22.5 (A), 42.7 (R)	40.9	0.11	30.6	0.07
C0.05	0.05	0.026	23.1 (A), 43.5 (R)	45.6	0.20	42.6	5
C0.25	0.25	0.16	23.6 (A), 43.5 (R)	43.4	0.21	43.8	9.4
C1	1	0.29	23.7 (A), 43.8 (R)	42.5	0.17	38.6	13.9
C2	2	0.42	24.0 (A), 44.1 (R)	43.9	0.18	38.6	10.3
C7	7	3.3	26.6 (A), 44.8 (R)	42.0	0.17	38.6	0.35
C100	100		5.1 ($Cu(OH)_2$)	82.1	0.33	55.0	0

[a] A and R denote anatase and rutile, respectively. ACS: Average crystallite size. [b] A and R denote anatase and rutile, respectively. PV: Pore volume.

experiment. The X-ray photoelectron spectroscopy (XPS) measurement was done in an ultra-high vacuum VG ESCALAB 210 electron spectrometer equipped with a multichannel detector. The spectra were excited using Mg Kα (1253.6 eV) radiation (operated at 200 W) of a twin anode in the constant analyser energy mode with a pass energy of 30 eV. Photoluminescence (PL) spectra were measured at room temperature on an F-7000 Fluorescence Spectrophotometer (Hitachi, Japan). The excitation wavelength was 300 nm, the scanning speed was 1200 nm min^{-1}, and the PMT voltage was 700 V. The widths of the excitation slit and emission slit were both 5.0 nm.

2.3 Photocatalytic hydrogen production

The photocatalytic hydrogen production experiments were performed in a 100 mL Pyrex flask at ambient temperature and atmospheric pressure, and the openings of the flask were sealed with silicone rubber septums. Four low power UV-LEDs (3 W, 365 nm) (Shenzhen LAMPLIC Science Co. Ltd. China), which were positioned 1 cm away from the reactor in four different directions, were used as light sources to trigger the photocatalytic reaction. The focused intensity and areas on the flask for each UV-LED was *ca.* 80.0 mW cm^{-2} and 1 cm^2, respectively. In a typical photocatalytic experiment, 50 mg of $Cu(OH)_2/TiO_2$ photocatalyst was suspended in 80 mL mixed solution of 0.09 M ethylene glycol and water. Prior to irradiation, the suspension of the catalyst was dispersed by an ultrasonic bath for 10 min, and then bubbled with nitrogen through the reactor for 40 min to completely remove the dissolved oxygen and ensure the reactor was in an anaerobic condition. A continuous magnetic stirrer was applied at the bottom of the reactor in order to keep the photocatalyst particles in suspension status during the whole experiments. A 0.4 mL gas was intermittently sampled through the septum, and hydrogen was analyzed by gas chromatography (GC-14C, Shimadzu, Japan, TCD, with nitrogen as a carrier gas and 5 Å molecular sieve column). All glassware was carefully rinsed with deionized water prior to use. The QE was measured and calculated according to eqn (1):

$$\mathrm{QE}[\%] = \frac{\text{number of reacted electrons}}{\text{number of incident photons}} \times 100 = \frac{\text{number of evolved } H_2 \text{ molecules} \times 2}{\text{number of incident photons}} \times 100 \quad (1)$$

The Chemical Oxygen Demand (COD) value before and after photocatalytic reaction was analyzed by the acidity potassium dichromate ($K_2Cr_2O_7$) method.

3. Results and discussion

3.1 Phase structures and morphology

XRD was used to identify and determine the phase structures and average crystallite size of the as-prepared samples. Fig. 1 shows XRD patterns of the C0, C0.05, C0.25, C1, C2, C7 and C100 ($Cu(OH)_2$) samples. It can be seen that only the anatase and rutile phases of TiO_2 were identified for pure TiO_2 (C0) and $Cu(OH)_2/TiO_2$ photocatalysts (C0.05, C0.25, C1, C2 and C7). No characteristic diffraction peaks of $Cu(OH)_2$ were observed because of its low loading content and weak crystallization. When $\boldsymbol{R} = 100$, six main diffraction peaks near or at $2\theta = 16.7$, 23.8, 34.1, 35.9, 39.8 and 53.2° can be observed, corresponding to (020), (021), (002), (111), (130) and (150) plane diffraction of $Cu(OH)_2$ [JCPDS No.12–420, Orthorrhombic, space group: Cmcm (63)], respectively. For all $Cu(OH)_2/TiO_2$ photocatalysts with different ***R***, characteristic diffraction peaks of anatase and rutile TiO_2 are observed, and there are no obvious changes of intensities and widths. This implies that there is no significant change observed in phase structure and crystallite size of TiO_2 during the whole precipitation. Also no evident shift in the peak positions is observed in each of the as-prepared $Cu(OH)_2/TiO_2$ samples, suggesting that the deposited $Cu(OH)_2$ clusters do not incorporate into the lattice of TiO_2, and are probably attached on the surface of TiO_2 particles.

The average crystallite size of anatase, rutile and $Cu(OH)_2$, calculated from the main diffraction peaks of anatase (101),

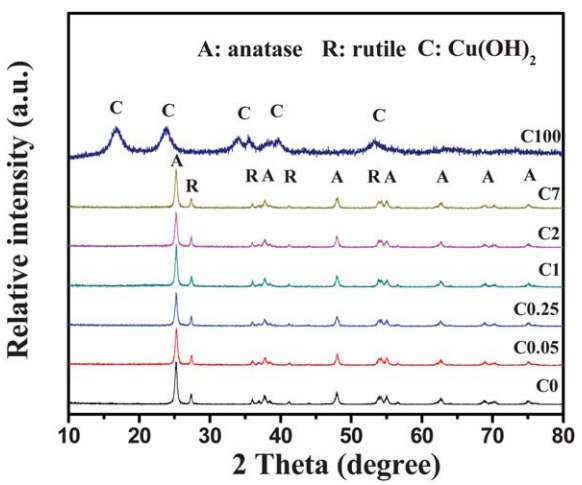

Fig. 1 XRD patterns of the samples C0, C0.05, C0.25, C1, C2, C7 and C100.

rutile (110) and $Cu(OH)_2$ (021) using Scherrer's equation, are listed in Table 1. All $Cu(OH)_2/TiO_2$ samples have almost the same crystallite size (*ca.* 23 nm for anatase, 44 nm for rutile), indicating that the deposition of $Cu(OH)_2$ clusters on the surface of TiO_2 has no obvious influence on its crystallite size and morphology. This is ascribed to the fact that ambient temperature deposition of $Cu(OH)_2$ does not have enough energy to stimulate the growth of TiO_2 crystal.[42] TEM was further used to observe the morphology and microstructures of as-prepared samples. Fig. 2 shows a typical TEM image of $Cu(OH)_2/TiO_2$ (sample C1). Many small $Cu(OH)_2$ clusters with size of *ca.* 1–3 nm can be clearly observed in Fig. 2. These small $Cu(OH)_2$ clusters are uniformly dispersed on the surface of the TiO_2 nanoparticles.

3.2 UV-Vis diffuse reflection spectra

Fig. 3 shows the UV-vis diffuse reflectance spectra of the bare TiO_2 and $Cu(OH)_2/TiO_2$ photocatalysts. As shown in the Figure, the absorption intensity of TiO_2 starts to increase at ~410 nm, corresponding to the intrinsic band gap absorption of rutile TiO_2, indicating a band gap of 3.0 eV, which coincides with the value reported in the literature.[43] As for $Cu(OH)_2/TiO_2$, the spectra show absorption in the ~700–800 nm region and an absorption shoulder at ~450 nm, in addition to the onset of absorption at ~410 nm. The 700–800 nm absorption can be assigned to the Cu(II) d–d transition.[43] In fact, the spectrum of the $Cu(NO_3)_2$ aqueous solution shows absorption centered at ~700–800 nm (inset of Fig. 3). Irie *et al.* have ascribed the absorption at ~450 nm of $Cu(OH)_2/TiO_2$ to the direct interfacial charge transfer (IFCT) from the VB of TiO_2 to Cu(II).[43] The absorption at ~450 and 700–800 nm increased with increasing amounts of the deposited $Cu(OH)_2$. In comparison to pure TiO_2 (C0), no great change in the absorption edge of the $Cu(OH)_2/TiO_2$ samples was observed, also implying that $Cu(OH)_2$ was not incorporated into the lattice of TiO_2, only deposited on its surface.

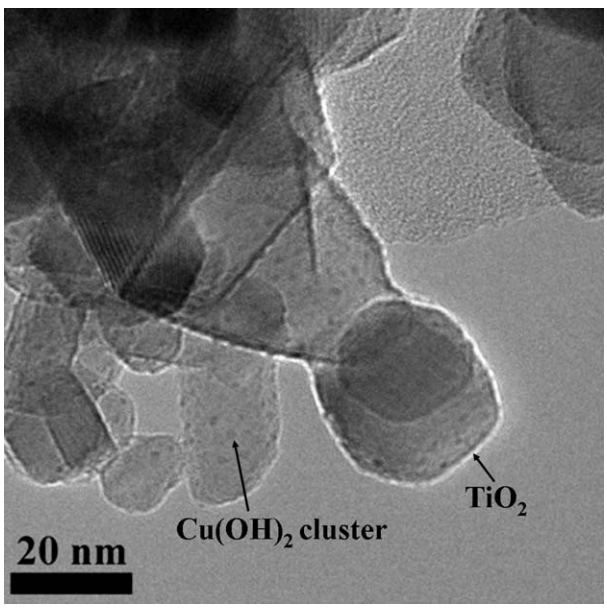

Fig. 2 High-magnification TEM images of sample C1.

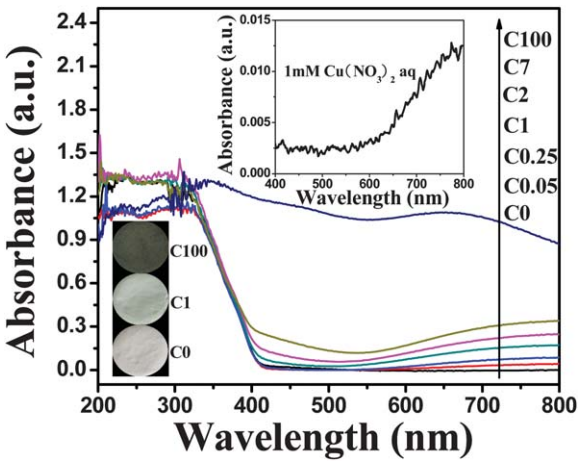

Fig. 3 UV-vis diffuse reflection spectra of C0, C0.05, C0.25, C1, C2, C7 and C100. The insets show the UV-vis absorption spectrum of 1 mM $Cu(NO_3)_2$ aqueous solution and the colors of C0, C1 and C100.

3.3 Band gap level analysis

For effective photocatalytic H_2-production, the conduction band edge of a semiconductor photocatalyst should be more negative than the H^+/H_2 potential. Therefore, it is of great importance to determine the band edges, especially the conduction band edge level of a semiconductor photocatalyst. Herein, the band edge positions of the conduction band and valence band of a semiconductor can be determined by a simple approach.[44,45,46] The conduction band edge (E_{CB}) of a semiconductor at the point of zero charge (pHzpc) can be determined by the following equation:

$$E_{CB} = \chi - E^e - 1/2E_g \quad (2)$$

where E_{CB} is the conduction band edge potential, χ is the electronegativity of the semiconductor, expressed as the geometric mean of the absolute electronegativity of the constituent atoms, which is defined as the arithmetic mean of the atomic electron affinity and the first ionization energy. E^e is the energy of free electrons on the hydrogen scale *ca.* 4.5 eV. E_g is the band gap of the semiconductor. The calculated conduction band position of anatase TiO_2 at the point of zero is about −0.26 eV, which is more negative than the H^+/H_2 reduction potential. This indicates that the photogenerated electrons on the conduction band of TiO_2 could energetically reduce the H^+ to produce H_2.

3.4 BET surface areas and pore size distributions

Usually, photocatalysts with higher specific surface areas and bigger pore volumes are beneficial for the enhancement of photocatalytic performance due to there being more surface active sites for the adsorption of reactant molecules, ease of transportation of reactant molecules and products through the interconnected porous networks, and enhanced harvesting of light.[12] Therefore, the effects of $Cu(OH)_2$ loading on the pore structure and BET surface areas of as-prepared samples are investigated by the adsorption–desorption measurement. Fig. 4 shows the nitrogen adsorption/desorption isotherms and the corresponding pore-size distribution curves (inset) of C0 and C1.

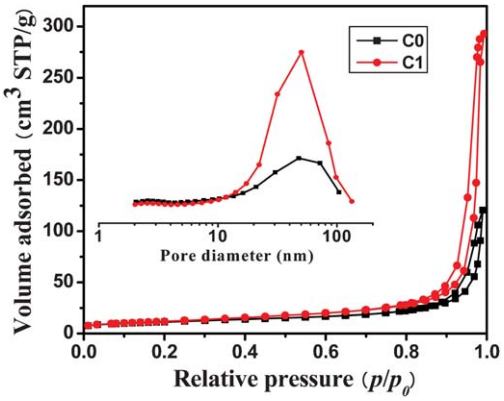

Fig. 4 Nitrogen adsorption–desorption isotherms and the corresponding pore-size distribution curves (inset) of C0 and C1.

It can be seen from Fig. 4 that the pure TiO_2 (C0) and $Cu(OH)_2/TiO_2$ (C1) samples have isotherms of type IV from the Brunauer–Deming–Deming–Teller (BDDT) classification, indicating the presence of mesopores (2–50 nm).[12,47–49] The shapes of the hysteresis loops are of type H3 at a high relative pressure range of 0.8 to 1.0, indicating the presence of slit-like pores. The isotherms show high absorption at a high relative pressure (P/P_0) range (approaching 1.0), implying the formation of large mesopores and macropores.[12,47–49] Further observation shows that the isotherms of C1 shift up compared to C0, suggesting C1 with higher surface areas. The pore size distribution curves (see inset of Fig. 4) calculated from the desorption branch of the nitrogen isotherms by the BJH method show a wide range of 2–103 nm with a peak pore diameter of about 50 nm for sample C0 and 2–133 nm with a peak pore diameter of about 48 nm for sample C1, further confirming the presence of mesopores and macropores.[47]

Table 1 shows quantitative details on BET surface area, pore volume and porosity of TiO_2 and $Cu(OH)_2/TiO_2$ samples. The $Cu(OH)_2/TiO_2$ samples show an increase in specific surface areas, pore volume and porosity compared with pure TiO_2, which can be ascribed to an increased formation of TiO_2 crystallite aggregates.

3.5 XPS analysis

To analyze the chemical composition of the prepared samples, and to identify the chemical status of Cu element in the samples, XPS analysis was carried out. The XPS survey spectrum (not shown here) of C1 indicates that Ti, O, Cu and C elements are observed and the corresponding photoelectron peaks appear respectively at binding energies of 458 (Ti2p), 530 (O1s), 932 (Cu2p) and 285 eV (C1s). The atomic ratio of Ti to O is about 1 : 2, which is in good accordance with the nominal atomic composition of TiO_2. The Cu peaks come from $Cu(OH)_2$. The C element is visible due to the residual carbon from the sample and adventitious hydrocarbon present in the XPS instrument itself.

Fig. 5 shows the comparison of high-resolution XPS spectra of Cu in the 2p region for samples $Cu(OH)_2$, C1, and C1 after photocatalytic reaction for 5 h. For $Cu(OH)_2$, the measured binding energies of Cu $2p_{3/2}$ and Cu $2p_{1/2}$ are equal to 935.3 and 955.2 eV, respectively. Meanwhile, two shake-up lines located at 944.1 and 963.0 eV are clearly observed, which is indicative of the

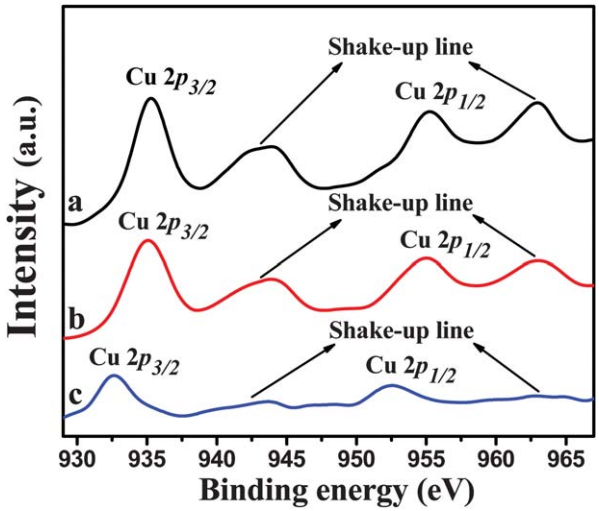

Fig. 5 High-resolution XPS spectra of Cu 2p of samples (a) pure $Cu(OH)_2$ (C100), (b) C1 and (c) C1 after 5 h photocatalytic hydrogen production from ethylene glycol aqueous solution under UV-LED irradiation.

paramagnetic chemical state of Cu^{2+}.[50] The XPS spectrum of sample C1 also shows typical Cu $2p_{3/2}$ and Cu $2p_{1/2}$ peaks with the measured binding energy of 935.1 and 955.0 eV, respectively, as well as their concomitant shake-up lines at 944.1 and 963.0 eV. The above XPS result can convincingly confirm the +2 oxidation state of copper existing on the surface of TiO_2 (for the as-prepared C1). This is also in good agreement with the above XRD and UV-visible measurement results and reports from Irie *et al.*[43] However, after the 5 h photocatalytic reaction, the XPS spectrum of sample C1 exhibits a significant change. Two shake-up lines almost disappear and the binding energies of Cu $2p_{3/2}$ and Cu $2p_{1/2}$ shift to 932.7 and 952.6 eV, respectively, indicating the formation of metal Cu due to the reaction of photo-generated electrons.[50] This also confirms the electron transfer from the CB of TiO_2 to $Cu(OH)_2$.

3.6 PL spectra

The PL emission spectra were used to investigate the efficiency of charge carrier trapping, immigration, transfer and separation, and to understand the fate of photogenerated electrons and holes in the semiconductor since PL emission results from the recombination of free carriers.[14,51,52] Fig. 6 presents a comparison of the PL spectra of samples C0 and C1 in the wavelength range of 350–550 nm. A fluorescence decrease (or quenching) is observed for $Cu(OH)_2/TiO_2$. The PL spectrum of pure TiO_2 (C0) is similar to that of the $Cu(OH)_2/TiO_2$ photocatalyst (C1). For the two samples, three main emission peaks appear at about 409, 451 and 468 nm, which were equivalent to 3.03, 2.75 and 2.65 eV, respectively. One of the major emission peaks at about 411 nm is ascribed to the interband PL phenomenon with the energy of light approximately equal to the band gap energy of rutile. The PL peaks at 451 and 468 nm are attributed to band edge free excitons. In addition, there are four small peaks observed in the wavelength range 480 to 550 nm. These PL signals are attributed to excitonic PL, which mainly results from surface oxygen vacancies or defects of the $Cu(OH)_2/TiO_2$ photocatalysts.[14,52]

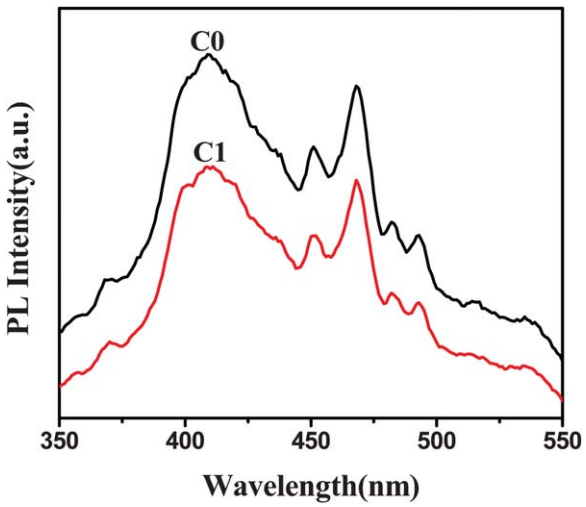

Fig. 6 Comparison of the photoluminescence spectra of samples C0 and C1.

The PL intensity of $Cu(OH)_2/TiO_2$ exhibits a decrease compared with pure TiO_2. This implies that $Cu(OH)_2/TiO_2$ has a lower recombination rate of electrons and holes under UV light irradiation. This is ascribed to the fact that the electrons are excited from the valence band to the conduction band of TiO_2 and then migrate to $Cu(OH)_2$ clusters, which prevent the direct recombination of electrons and holes.

3.7 Photocatalytic activity

Photocatalytic H_2-production activity on various samples was evaluated under UV-LED irradiation using ethylene glycerol as a scavenger.[32–35] Control experiments indicated that no appreciable hydrogen production was detected in the absence of either irradiation or photocatalyst, suggesting that hydrogen was produced by photocatalytic reactions on photocatalyst. Fig. 7 presents the comparison of the photocatalytic H_2-production activity of TiO_2 and $Cu(OH)_2/TiO_2$ samples. ***R*** exhibits a significant influence on the photocatalytic activity. For C0, it shows

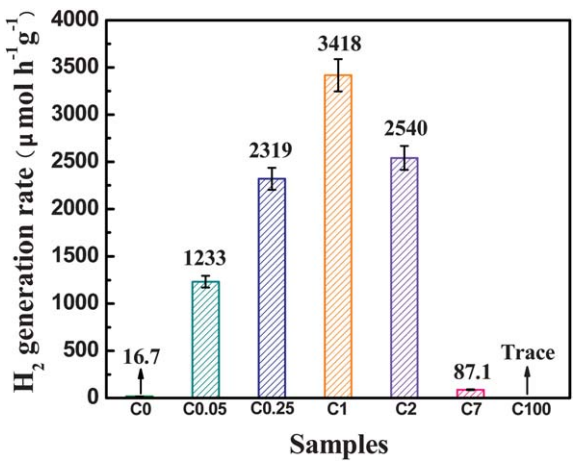

Fig. 7 Comparison of the photocatalytic activity of C0, C0.05, C0.25, C1, C2, C7 and C100 for the photocatalytic H_2-production from ethylene glycol aqueous solution under UV-LEDs irradiation.

a very low photocatalytic activity because of the rapid recombination between CB electrons and VB holes in pure TiO_2 and the presence of a large overpotential in the production of H_2. After loading only a small amount of $Cu(OH)_2$ clusters, the activity of C0.05 is remarkably improved. The photocatalytic activity of the samples further increased with increasing ***R*** from 0.05 to 1. The highest H_2-production rate, obtained for sample C1, is 3418 μmol h^{-1} g^{-1}, with 13.9% QE. This value exceeds that of pure TiO_2 (C0) by a factor of 205. At $\boldsymbol{R}_{Cu} > 1$, a further increase in $Cu(OH)_2$ content leads to a reduction of the photocatalytic activity. Especially at $\boldsymbol{R}_{Cu} = 7$, the photocatalytic activity of C7 has a drastic decrease. This is probably due to the combined effects of following factors: (i) the decrease (or shielding) of the TiO_2 surface active sites due to deposition of excessive $Cu(OH)_2$ clusters; (ii) deterioration of the catalytic properties of $Cu(OH)_2$ clusters or disappearance of surface effect due to the increase of their particle size;[53,54] (iii) increase in the opacity leading to a decrease of irradiation passing through the reaction suspension solution.[55] No hydrogen can be detected when $Cu(OH)_2$ alone is used as the catalyst, suggesting that pure $Cu(OH)_2$ was not active for photocatalytic H_2 production under the experimental conditions studied.

From what has been observed and discussed above, we can draw several important conclusions: (1) The TiO_2 without $Cu(OH)_2$ cluster modification is inactive for photocatalytic hydrogen generation under UV light irradiation, although the conduction band level of anatase TiO_2 is more negative than the reduction potential of H^+/H_2. (2) After $Cu(OH)_2$ cluster modification, the photocatalytic activity of samples can be greatly enhanced. (3) The H_2-production activity of $Cu(OH)_2$ cluster-modified TiO_2 can be controlled by tuning the $Cu(OH)_2$ content. Based on the above results, the photocatalytic mechanisms are proposed in Fig. 8. Although the conduction band edge of anatase is higher (or more negative) than the reduction potential of H^+/H_2, the rate of H_2 generation was negligible over bare TiO_2 without $Cu(OH)_2$ clusters. This can be understood by considering the rapid recombination rate of CB electrons and VB holes and the presence of a large H_2-production overpotential in pure TiO_2. Once the sample was modified with $Cu(OH)_2$, the potential of $Cu(OH)_2/Cu$ was about −0. 224 V (vs SHE, pH = 0);[56] thus, it can be expected to act as a co-catalyst to reduce protons efficiently ($E^0_{H+/H2} = 0$ V *vs.* SHE, pH = 0). Therefore, under UV light irradiation, the VB electrons of TiO_2 are excited to CB. Because the potential (−0.224 V *vs.* SHE, pH = 0)) of $Cu(OH)_2/Cu$ is slightly lower than the CB level (about −0.26 V) of anatase TiO_2, the photoinduced electrons in the CB can be further transferred to $Cu(OH)_2$ clusters and then effectively reduce protons to produce H_2 molecules. This also retards the recombination of photoinduced electrons and holes. Consequently, high photocatalytic H_2-production activity is achieved over TiO_2 samples as a result of surface $Cu(OH)_2$ modification. However the holes in the VB cause the decomposition of sacrificial reagent ethylene glycol. Therefore, it is not surprising that when ***R*** is lower than 1, with increasing $Cu(OH)_2$ content, more $Cu(OH)_2$ clusters are deposited on the TiO_2 surface, resulting in the increase of the activity. On the contrary, when ***R*** is higher than 1, with further increasing $Cu(OH)_2$ content, the particle size of the $Cu(OH)_2$ clusters increases, the surface effect becomes weak or disappears, causing the reduction of the photocatalytic activity.

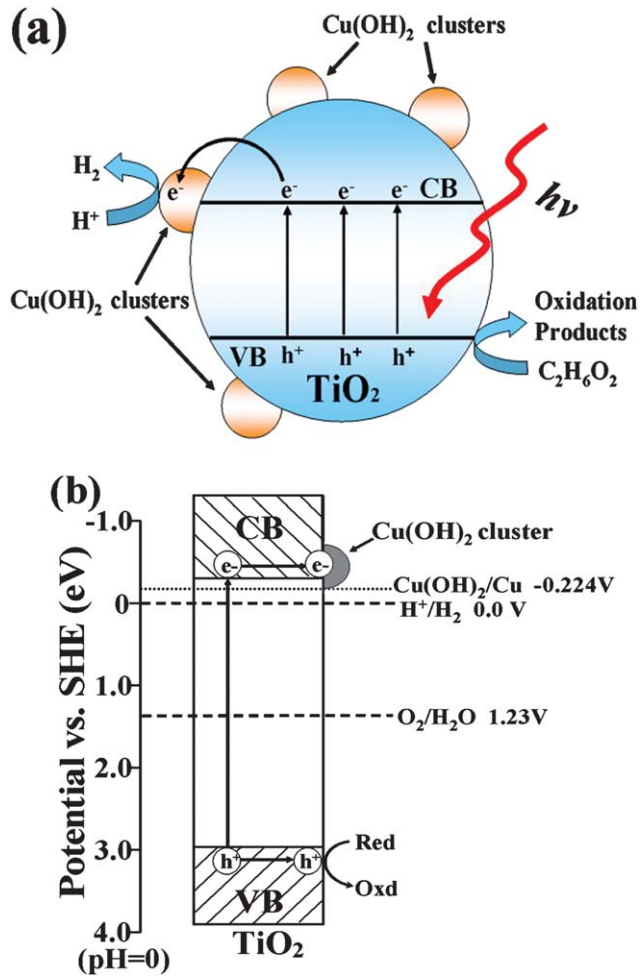

Fig. 8 (a) Schematic illustration for the charge transfer and separation in the $Cu(OH)_2$ cluster-modified TiO_2 system under UV-LED irradiation. (b) Proposed mechanism for photocatalytic H_2-production under UV light irradiation.

The above fluorescence quenching experiments further confirm the transfer of photogenerated electrons from TiO_2 to $Cu(OH)_2$ clusters and the favorable (or close) contact between $Cu(OH)_2$ cluster and TiO_2 nanoparticles. It should be to be noted that at the beginning, the transferred electrons from TiO_2 CB to $Cu(OH)_2$ clusters will cause the reduction of partial Cu^{2+} to Cu^0 atoms, and then the formation of Cu clusters. These Cu clusters can work as a co-catalyst to promote the separation and transfer of photo-generated electrons from the TiO_2 CB to the $Cu(OH)_2$/Cu cluster, where H^+ is reduced to hydrogen molecules. The major reaction steps in this photocatalytic mechanism under UV light irradiation are summarized by eqn (3) and (4).

$$Cu(OH)_2 + 2e^- = Cu + 2OH^- \quad (3)$$

$$Cu + 2e^- + 2H^+ = Cu + H_2 \quad (4)$$

To confirm the fact that the photocatalytic hydrogen production was accompanied by the degradation of ethylene glycol, the COD value, reflecting the level of organic pollutant concentration, was measured in the presence of C1. Fig. 9 shows the COD value of the solution and the amount of hydrogen production as a function of photocatalytic reaction time under UV-LED irradiation over the sample C1 from a 5.9 mM ethylene glycol aqueous solution. The initial COD value of the ethylene glycol aqueous solution was 469 mg L^{-1}; with increasing irradiation time, this value decreased to 287 mg L^{-1}, while the amount of hydrogen production increased significantly from 0 to 3762 μmol g^{-1} after 6 h of light irradiation. The reduction of the H^+ and the degradation of ethylene glycol occurred simultaneously. To further test the repeatability of photocatalytic H_2-production on sample C1, we carried out the photocatalytic H_2-production experiment repeatedly five times (not shown here). The photocatalyst is stable under repeated application with nearly constant H_2-production rate, showing that sample C1 was not deactivated during the photocatalytic H_2-production.

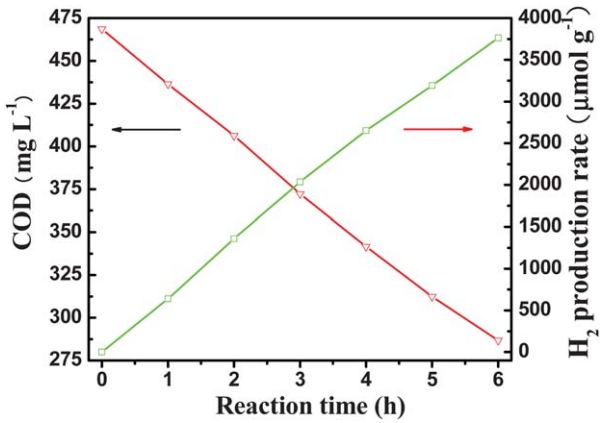

Fig. 9 The COD value for the reaction solution and the amount of H_2-production as a function of irradiation time over sample C1 under UV-LED irradiation.

4. Conclusions

In summary, we have successfully developed a simple precipitation method to fabricate highly active $Cu(OH)_2$ cluster-modified TiO_2 photocatalysts for photocatalytic H_2 production. $Cu(OH)_2$ clusters are effective co-catalysts to enhance the photocatalytic H_2-production activity of TiO_2, and its content exhibits a significant influence on the activity. The optimal $Cu(OH)_2$ loading content is determined to be 0.29 mol%, and the corresponding hydrogen production rate is 3418 μmol h^{-1} g^{-1} with a QE of 13.9%, which exceeds that of pure TiO_2 by more than 205 times. The potential of $Cu(OH)_2$/Cu are deemed to be lower than the conduction band of TiO_2 and more negative than the H^+/H_2 potential, which favors the electron transfer from the CB of TiO_2 to $Cu(OH)_2$ and the reduction of H^+, thus enhancing photocatalytic H_2-production activity. This work not only shows a possibility for the utilization of low cost $Cu(OH)_2$ clusters as a substitute for noble metals in photocatalytic hydrogen production, but also exhibits a facile method for fabricating highly active H_2-production photocatalysts by a simple precipitation reaction.

Acknowledgements

This work was partially supported by the National Natural Science Foundation of China (50625208, 20773097, 20877061

and 51072154) and the Natural Science Foundation of Hubei Province (2010CDA078). This work was also financially supported by the National Basic Research Program of China (2007CB613302).

References

1 S. P. Xu and D. D. Sun, *Int. J. Hydrogen Energy*, 2009, **34**, 6096.
2 Y. Q. Wu, G. X. Lu and S. B. Li, *J. Phys. Chem. C*, 2009, **113**, 9950.
3 A. Fujishima and K. Honda, *Nature*, 1972, **238**, 37.
4 J. G. Yu, L. F. Qi and M. Jaroniec, *J. Phys. Chem. C*, 2010, **114**, 13118.
5 M. R. Hoffmann, S. T. Martin, W. Choi and D. W. Bahnemann, *Chem. Rev.*, 1995, **95**, 69.
6 J. G. Yu, Q. J. Xiang, J. R. Ran and S. Mann, *CrystEngComm*, 2010, **12**, 872.
7 Z. G. Zou, J. H. Ye, K. Sayama and H. Arakawa, *Nature*, 2001, **414**, 625.
8 R. Asahi, T. Morikawa, T. Ohwaki, K. Aoki and Y. Taga, *Science*, 2001, **293**, 269.
9 S. W. Liu, J. G. Yu and M. Jaroniec, *J. Am. Chem. Soc.*, 2010, **132**, 11914.
10 M. Ni, M. K. H. Leung, D. Y. C. Leung and K. Sumathy, *Renewable Sustainable Energy Rev.*, 2007, **11**, 401.
11 Y. X. Li, G. X. Lu and S. B. Li, *J. Photochem. Photobiol., A*, 2002, **152**, 219.
12 J. G. Yu, Y. R. Su and B. Cheng, *Adv. Funct. Mater.*, 2007, **17**, 1984.
13 A. A. Nada, M. H. Barakat, H. A. Hamed, N. R. Mohamed and T. N. Veziroglu, *Int. J. Hydrogen Energy*, 2005, **30**, 687.
14 J. C. Yu, J. G. Yu, W. K. Ho, Z. T. Jiang and L. Z. Zhang, *Chem. Mater.*, 2002, **14**, 3808.
15 J. Bandara, C. P. K. Udawattab and C. S. K. Rajapaksea, *Photochem. Photobiol. Sci.*, 2005, **4**, 857.
16 T. Sreethawong and S. Yoshikawa, *Int. J. Hydrogen Energy*, 2006, **31**, 786.
17 M. Jakob, H. Levanon and P. V. Kamat, *Nano Lett.*, 2003, **3**, 353.
18 N. L. Wu and M. S. Lee, *Int. J. Hydrogen Energy*, 2004, **29**, 1601.
19 A. Galinska and J. Walendziewski, *Energy Fuels*, 2005, **19**, 1143.
20 J. G. Yu, Q. J. Xiang and M. H. Zhou, *Appl. Catal., B*, 2009, **90**, 595.
21 W. Choi, A. Termin and M. R. Hoffmann, *J. Phys. Chem.*, 1994, **98**, 13669.
22 M. L. Litter, *Appl. Catal., B*, 1999, **23**, 89.
23 S. U. M. Khan, M. Al-Shahry and W. B. Ingler, *Science*, 2002, **297**, 2243.
24 Y. X. Li, G. F. Ma, S. Q. Peng, G. X. Lu and S. B. Li, *Appl. Surf. Sci.*, 2008, **254**, 6831.
25 Z. L. Jin, X. J. Zhang, Y. X. Li, S. B. Li and G. X. Lu, *Catal. Commun.*, 2007, **8**, 1267.
26 R. Abe, K. Sayama and H. Arakawa, *Chem. Phys. Lett.*, 2002, **362**, 441.
27 N. Alonso-Vante, H. Colell and H. Tributsch, *J. Phys. Chem.*, 1993, **97**, 7381.
28 S. G. Lee, S. W. Lee and H. I. Lee, *Appl. Catal., A*, 2001, **207**, 173.
29 B. Zielinska, E. Borowiak-Palen and R. J. Kalenczuk, *Int. J. Hydrogen Energy*, 2008, **33**, 1797.
30 S. Kim and W. Choi, *J. Phys. Chem. B*, 2002, **106**, 13311.
31 V. Subramanian, E. E. Wolf and P. Kamat, *J. Am. Chem. Soc.*, 2004, **126**, 4943.
32 B. D. Mcginnis, V. D. Adams and E. J. Middlebrooks, *Water Res.*, 2000, **34**, 2346.
33 D. Carnegie and J. A. Ramsay, *Biodegradation*, 2009, **20**, 551.
34 B. D. Mcginnis, V. D. Adams and E. J. Middlebrooks, *Chemosphere*, 2001, **45**, 101.
35 G. R. Bamwenda, S. Tsubota, T. Kobayashi and M. Haruta, *J. Photochem. Photobiol., A*, 1994, **77**, 59.
36 S. Sakthivel, M. V. Shankar, M. Palanichamy, B. Arabindoo, D. W. Bahnemann and V. Murugesan, *Water Res.*, 2004, **38**, 3001.
37 L. S. Yoong, F. K. Chong and K. D. Binay, *Energy*, 2009, **34**, 1652.
38 V. Gombac, L. Sordelli, T. Montini, J. D. Juan, A. Adamski, G. Adami, M. Cargnello, S. Bernal and P. Fornasiero, *J. Phys. Chem. A*, 2010, **114**, 3916.
39 T. Sreethawong and S. Yoshikawa, *Catal. Commun.*, 2005, **6**, 661.
40 H. J. Choi and M. Kang, *Int. J. Hydrogen Energy*, 2007, **32**, 3841.
41 S. P. Xu, J. W. Ng, X. W. Zhang, H. W. Bai and D. D. Sun, *Int. J. Hydrogen Energy*, 2010, **35**, 5254.
42 (*a*) J. G. Yu and B. Wang, *Appl. Catal., B*, 2010, **94**, 295; (*b*) J. G. Yu, S. W. Liu and M. H. Zhou, *J. Phys. Chem. C*, 2008, **112**, 2050.
43 (*a*) X. Qiu, M. Miyauchi, H. Yu, H. Irie and K. Hashimoto, *J. Am. Chem. Soc.*, 2010, **132**, 15259; (*b*) H. Yu, H. Irie and K. Hashimoto, *J. Am. Chem. Soc.*, 2010, **132**, 6898; (*c*) H. Irie, S. Miura, K. Kamiya and K. Hashimoto, *Chem. Phys. Lett.*, 2008, **457**, 202; (*d*) H. Irie, K. Kamiya, T. Shibanuma, S. Miura, D. A. Tryk, T. Yokoyama and K. Hashimoto, *J. Phys. Chem. C*, 2009, **113**, 10761.
44 L. Ge, *Mater. Chem. Phys.*, 2008, **107**, 465.
45 H. Xu, H. Li, C. Wu, J. Chu, Y. Yan, H. Shu and Z. Gu, *J. Hazard. Mater.*, 2008, **153**, 877.
46 H. Q. Jiang, H. Endo, H. Natori, M. Nagai and K. Kobayashi, *Mater. Res. Bull.*, 2009, **44**, 700.
47 K. S. W. Sing, D. H. Everett, R. A. W. Haul, L. Moscou, R. A. Pierotti, J. Rouquerol and T. Siemieniewska, *Pure Appl. Chem.*, 1985, **57**, 603.
48 J. G. Yu, W. G. Wang, B. Cheng and B. L. Su, *J. Phys. Chem. C*, 2009, **113**, 6743.
49 J. G. Yu, J. C. Yu, M. K. P. Leung, W. K. Ho, B. Cheng, X. J. Zhao and J. C. Zhao, *J. Catal.*, 2003, **217**, 69.
50 *Handbook of X-ray Photoelectron Spectroscopy*, ed. J. F. Moulder, W. F. Stickle, P. E. Sobol, K. D. Bomben, J. Chastain, Physical Electronics, Inc., Eden Prairie, MN, 1992.
51 W. F. Zhang, M. S. Zhang, Z. Yin and Q. Chen, *Appl. Phys. B: Lasers Opt.*, 2000, **70**, 261.
52 J. G. Yu, L. Yue, S. W. Liu, B. B. Huang and X. Y. Zhang, *J. Colloid Interface Sci.*, 2009, **334**, 58.
53 W. K. Ho, J. C. Yu, J. Lin, J. G. Yu and P. Li, *Langmuir*, 2004, **20**, 5865.
54 J. G. Yu, J. Zhang and M. Jaroniec, *Green Chem.*, 2010, **12**, 1611.
55 J. G. Yu, X. J. Zhao and Q. N. Zhao, *Thin Solid Films*, 2000, **379**, 7.
56 *Standard Potentials in Aqueous Solution*, ed. A. J. Bard, R. Parsons, J. Jordan, Marcel Dekker, New York, 1985.